Published in final edited form as:
Pharm Res. 2012 November ; 29(11): 3090–3101. doi:10.1007/s11095-012-0801-x.

Phospho-sulindac (OXT-328) Inhibits the Growth of Human Lung Cancer Xenografts in Mice: Enhanced Efficacy and Mitochondria Targeting by Its Formulation in Solid Lipid Nanoparticles

Rongrong Zhu, **Ka-Wing Cheng**, **Gerardo Mackenzie**, **Liqun Huang**, **Yu Sun**, **Gang Xie**, **Kveta Vrankova**, and **Basil Rigas**
Division of Cancer Prevention, Department of Medicine, Stony Brook University, Stony Brook, New York

Panayiotis P. Constantinides
Medicon Pharmaceuticals, Inc., Stony Brook, New York

Abstract

Purpose—To evaluate the antitumor efficacy of solid lipid nanoparticle–encapsulated phospho-sulindac (SLN-PS) in human lung cancer.

Methods—PS was incorporated into SLNs using the emulsion evaporation technique. We determined the antitumor activity of SLN-PS in cultured lung cancer cells. The performance of SLN-PS was further evaluated by pharmacokinetic studies in mice and in a model of human lung cancer xenografts in nude mice.

Results—SLN-PS was >4-fold more potent than PS in inhibiting the growth of A549 and H510 cells *in vitro*. SLN-PS enhanced cellular uptake and facilitated PS accumulation in mitochondria, leading to oxidative stress and apoptosis via the mitochondrial-apoptosis pathway. SLN-PS was highly effective in suppressing the growth of A549 xenografts (78% inhibition compared to control, $p < 0.01$); while PS had no significant effect. Formulation of PS in SLNs resulted in improved pharmacokinetics in mice and an enhanced (~14-fold) accumulation of PS and its metabolites in A549 xenografts. Finally, SLN-PS enhanced urinary F2-isoprostane uniquely in mice bearing A549 xenografts compared to untreated controls, suggesting that SLN-PS specifically induced oxidative stress in tumors.

Conclusions—Our results show that SLN-PS is efficacious in suppressing the growth of lung cancer and merits further evaluation.

Keywords

lung cancer; mitochondria targeting; non-steroidal anti-inflammatory drugs; phospho-sulindac; solid lipid nanoparticles

INTRODUCTION

Lung cancer is the leading cause of cancer-related deaths worldwide. Despite advances in early detection and chemotherapy, lung cancer still has a 5-year survival <15% (1). It is clear that new agents against lung cancer are urgently needed.

Corresponding author: Basil Rigas Division of Cancer Prevention, HSC, T-17 Room 080, Stony Brook, NY 11794-8173 Tel: 631-444-9538; Fax: 631-444-9553; basil.rigas@stonybrook.edu.

Nonsteroidal anti-inflammatory drugs (NSAIDs) reduce the incidence of various cancers including lung cancer (2,3). Sulindac and sulindac sulfone have been shown to strongly inhibit lung tumorigenesis in mice, reducing lung tumor multiplicities by 52% and 71%, respectively (4,5). However, the long term use of sulindac is associated with significant gastrointestinal toxicity. We have synthesized phospho-sulindac (PS, OXT-328), a novel sulindac derivative, that shows considerable efficacy towards colon cancer and less gastrointestinal toxicity compared to the parent compound (6–10). However, PS is much more hydrophobic as reflected by its higher partition coefficient (logP, 3.91 vs 2.29), resulting in poor solubility in aqueous milieus. This property potentially limits the bioavailability of PS and thus its effective delivery to tumor site(s) *in vivo*.

Nanocarriers are emerging tools that have demonstrated great potential in the delivery of lipophilic drugs, by i) dissolution of drug in aqueous solution above their solubility limit, ii) stabilization of drug, iii) specific delivery to target site(s) and iv) overcoming multidrug resistance (11). Solid lipid nanoparticles (SLNs) are colloidal carriers which are being increasingly appreciated as alternative drug carrier systems to traditional polymeric nanoparticles (12,13). SLNs consist of a solid lipid core, in which lipophilic therapeutics, such as PS, could be efficiently entrapped and released in a controlled manner. SLNs have been reported to efficiently improve pharmacokinetic profile (14–16), targeted drug delivery to tumor sites and efficacy, while minimizing systemic side effects (17–19).

In this study, we formulated PS in SLNs, and showed that SLN-PS has potent anticancer activity towards non-small cell lung cancer (NSCLC) *in vitro* and in xenografts in mice. We also report on its pharmacokinetic properties and its novel mechanism of action against lung cancer.

MATERIALS AND METHODS

Reagents

Phospho-sulindac (OXT-328) was a gift from Medicon Pharmaceuticals, Inc, Setauket, NY. Its partition coefficient (LogP) between octanol and water was determined to be 3.91. Stearic acid, lecithin, chloroform, and Myrj59 were purchased from Sigma-Aldrich. Cell culture reagents were purchased from American Type Culture Collection.

SLN-PS Preparation

SLN-PS was prepared using an emulsion/evaporation technique. Briefly, 450 mg Myrj59 was dissolved in 60 ml deionized water. The aqueous solution was heated to 75 °C in a water bath under constant stirring at 700 rpm. The organic phase consisted of 380 mg stearic acid, 200 mg lecithin and 300 mg PS dissolved in 20 ml chloroform. The organic phase was gently injected into the aqueous phase with a syringe. The speed of the stirrer was then increased to 1000 rpm. After 2.5 h (when the volume of the emulsion was reduced to about 5–10 mL), 10 mL of ice-cold water was added and stirring continued for another 2 h at 1000 rpm. The resulting suspension was centrifuged at 7,200g for 1 h and the supernatant was discarded. The pellet was washed twice by re-suspending in deionized water followed by centrifugation to remove the supernatant. The final pellet was re-suspended in deionized water, frozen at −20 °C overnight, and freeze-dried.

Characterization of SLN-PS

The morphology of the SLN particles was determined by transmission electron microscopy. One mg SLN-PS was suspended in 2 mL phosphate buffered saline (PBS, pH 7.4) and one drop of the suspension was mounted onto a slide. The shape and size of the particles were then recorded.

To determine the entrapment efficiency of PS, freshly prepared colloidal samples (from the ice-water chilling step) were centrifuged and non-entrapped PS in the supernatant was determined by high-performance liquid chromatography (HPLC). The % entrapment efficiency of PS in SLNs was calculated using the following equation:

$$\%\ \text{entrapment efficiency} = (n1 - n2)/n1 * 100\%$$

where n1 = total amount of PS used; n2 = amount of free PS in the supernatant.

To determine the loading of PS in SLNs, 1.0 mg lyophilized SLN-PS was dissolved in 1.0 mL ethanol. After the appropriate dilution, HPLC analysis was performed to determine the percentage drug loading.

Release Profile of PS from SLNs *In Vitro*

Freshly prepared SLN-PS suspension samples were dialyzed against 100 ml PBS (pH 7.4) or F-12K cell culture medium under constant stirring at 300 rpm at 37 °C. At designated time points (Fig. 1), the dialysis buffer was replaced with fresh buffer. The cumulative percentage release of PS from SLNs was measured by HPLC and plotted against time. Triplicate experiments were performed.

Cell Culture and Cytokinetic Analysis

Human non-small cell lung cancer (A549, wild type p53) and small cell lung cancer (H510, mutant p53) cells were cultured as recommended by ATCC. Cell viability was measured with the MTT assay (Roche Diagnostics) and cell proliferation with the 5-bromo-2′-deoxyuridine (BrdU; BD Immunocytometry Systems) assay, according to the manufacturer's instructions. Apoptosis and necrosis were assessed by staining cells with Annexin V and propidium iodide and analyzing them by flow cytometry (20).

Uptake and Intracellular Distribution of SLN-PS

A549 cells were treated with 60 μM SLN-PS or PS, harvested at specified time points and washed with ice-cold PBS. Cell lysates were obtained by sonication. To analyze mitochondrial drug levels, mitochondria were isolated using the Mitochondria Isolation Kit (Thermo Scientific). Drug levels were then determined by HPLC and normalized to the protein content. Intracellular localization was also examined by confocal microscopy, using FITC-entrapped SLN-PS. A549 cells cultured in 35mm glass-bottomed microwell dishes (MatTek, Ashland MA) were treated with 60 μM SLN-PS-FITC or free FITC. At specified time points, the medium was aspirated, monolayers were washed twice with PBS and examined with a two-photon laser scanning confocal microscope (Zeiss LSM 510 META NLO).

Western Blot

Cell lysates were resolved by sodium dodecyl sulfate electrophoresis and transferred onto polyvinylidene difluoride membranes. Bad, Bid, caspase-9, caspase-3, caspase-7, caspase-8, cytochrome c and p-Bad antibodies (Cell Signaling Technology, Danvers, MA) were used. Loading control: β-actin.

Intracellular ROS and Mitochondrial Superoxide

After drug treatment, cells were trypsinized, incubated with 10 μM DCF-DA for 30 min at 37°C, and the fluorescence intensity was analyzed by flow cytometry (FACSCaliber, BD

Bioscience). To assay mitochondrial superoxide anion levels, cells were stained with 5 μM MitoSOX Red for 30 min at 37°C and analyzed on a FACSCaliber.

Trx-2 Overexpression

A549 cells seeded in 100-mm dishes were transfected with Trx-2 plasmid or the empty vector for 48 h using Lipofectamine 2000 (Invitrogen) according to the manufacturer's protocol.

Mitochondrial DNA Depleted Cells (ρ^0)

A549 cells depleted of mitochondrial DNA (ρ^0) were generated by incubating cells with 200 ng/ml ethidium bromide and 50 μg/ml uridine for 8 weeks as previously described (21).

Xenograft Tumor Model

A549 cells (2.5×10^6) in 100 μl PBS were injected subcutaneously in both left and right flanks of 5–6 week-old female Ncr nude mice (Taconic, Hudson, NY). When the average tumor volume reached 180 mm^3, the mice were treated with vehicle (PBS) or SLN-PS (300 mg/kg/day, i.p.) or PS (150 mg/kg, p.o.), for 5 d per week. Dosage of PS and SLN-PS was equivalent to 70% of their respectively MTD. Tumor size was monitored by measuring their length (L) and width (W) with a caliper, and tumor volume was calculated using the following formula: $L \times W \times (L + W/2) \times 0.56$. On day 10, an 18-h urine sample was collected from each mouse using individual metabolic cages. The mice were euthanized on day 22, one hour after drug administration. Blood and the major organs were collected. Tumors were divided into halves, one fixed in 10% buffered formalin and the other stored in liquid nitrogen. Xenograft mitochondria were isolated using a Mitochondria Isolation Kit for Tissues (Thermo Scientific).

Immunohistochemistry

Cell death and proliferation were determined in paraffin embedded tissue sections using the terminal deoxynucleotidyl transferase dUTP nick end labeling (TUNEL) and Ki-67 immunohistochemical staining, respectively, as previously described (20).

Urinary F-2 Isoprostane Analysis

Levels of F2-isoprostane and creatinine in urine of mice were determined by ELISA (Oxford Biomedical Research (Oxford, MA). F2-isoprostane values were normalized to creatinine levels.

Pharmacokinetics and Biodistribution

BALB/c female mice 5~6 wks old (Taconic, Hudson, NY) were treated with a single dose of PS or SLN-PS (50 mg/kg i.p. or p.o.). Mice were euthanized at designated time points and blood samples were collected by cardiac puncture. After centrifugation, plasma was extracted with acetonitrile. Tissues were homogenized, sonicated, and extracted with acetonitrile. The levels of PS and its main metabolites were determined by HPLC. The results were normalized to protein content.

Statistical Analyses

Data are expressed as mean ± S.E.M. Statistical analyses were performed by ANOVA. P values < 0.05 were considered statistically significant.

RESULTS

Characterization of SLN-PS

SLN-PS particles are round in shape, ranging from 20 to 100 nm in diameter (Fig.1). The entrapment efficiency and drug-loading capacity of SLN-PS were 72 ± 3% and 33 ± 2%, respectively. The release of PS from SLNs, essentially identical in PBS and F-12 cell culture medium, showed a burst during the first 3 h, reflecting the release of drug adsorbed on the surface of nanoparticles. About 42% of the drug was released by 24 h, 75% by 72 h and 98% by 120 h.

SLN-PS Inhibits the Growth of A549 Lung Cancer Cells and Alters Their Cytokinetics

We evaluated the effect of sulindac, PS and SLN-PS on the growth of two human lung cancer cell lines, A549 (non-small cell lung cancer) and H510 (small cell lung cancer). PS inhibited the growth of these cell lines >11–22 fold more potently than sulindac (Fig. 1, table). Cell death appeared to be p53-independent, as the growth inhibitory effect of PS was observed both in the p53 wild-type (A549) and p53 mutant (H510) cell lines. Incorporating PS into SLNs further enhanced its cell growth inhibitory effect, bringing the overall enhancement over sulindac to >44–111 fold. Of note, plain SLNs (no drug loaded) at concentrations equivalent to up to $3\times IC_{50}$ of SLN-PS did not appreciably affect cell growth.

The growth inhibitory effect of SLN-PS and PS results from their cytokinetic effect (Fig. 2). SLN-PS dose-dependently decreased cell proliferation, reaching a 52% reduction at its IC_{50} (Fig. 2A). Equimolar concentrations of PS unincorporated in SLNs had a weaker effect on proliferation (25% reduction), while plain SLNs had only a marginal effect (14% reduction). An equipotent concentration of PS (i.e. one that inhibited 50% of cell growth at 24 h) caused only a 37% reduction of proliferation. These findings indicate that PS, when incorporated into SLNs may have a somewhat different mode of action than PS by itself. At 24 h, SLN-PS increased apoptosis 7-fold compared to control (Fig. 2B). Interestingly, the effect of PS on apoptosis was marginal and of plain SLNs was modest, whereas the sum of the two effects was only 2-fold over control. The effect of an equipotent concentration of PS was about half that of SLN-PS.

Taken together, these findings indicate that SLN-PS has a distinctly more pronounced effect on apoptosis than on cell proliferation compared to PS, which may reflect different modes of action between the two formulations of PS.

SLN-PS Activates the Intrinsic Apoptosis Pathway

Mitochondria are central to cell survival and death (22). SLN-PS activated procaspase 9 but not procaspase 8 (Fig. 2D), suggesting that it induced apoptosis through the intrinsic (mitochondrial) pathway. Collapse of mitochondrial transmembrane potential ($\Delta\psi m$) is a key event in mitochondria-mediated apoptosis. We evaluated $\Delta\psi m$ using the molecular marker JC-1; increased JC-1 green fluorescence indicates decreased $\Delta\psi m$.

SLN-PS dissipated $\Delta\psi m$ potently, increasing JC-1 green fluorescence by nearly 13-fold compared to the control (Fig. 2C). In contrast, an equimolar concentration of PS had no effect on $\Delta\psi m$, whereas an equipotent concentration of PS increased JC-1 fluorescence by only 2.8-fold. Plain SLNs without PS increased JC-1 fluorescence by 5-fold. SLN-PS is thus considerably more effective in inducing $\Delta\psi m$ dissipation than PS.

Downstream of $\Delta\psi m$ dissipation, SLN-PS caused the release of cytochrome c and the subsequent activation of cell death signaling molecules such as caspase 3 and caspase 7. These effects are time-dependent, evident as early as 1 h post treatment; they also manifest

the appropriate temporal sequence (Fig. 2D). The lack of an effect by SLN-PS on Bid and Bad (both upstream of caspase 9) suggests that SLN-PS likely targets the mitochondria directly, leading to activation of caspase 9.

SLN-PS Increases the Levels of Intracellular RONS and Mitochondrial Superoxide Anion: Differential Cellular Uptake and Mitochondrial Targeting

We have previously demonstrated that PS and similar agents induce RONS, an effect that may mediate their anticancer activity (23); mitochondria are the main source of cellular RONS (23). Therefore, we explored the effect of SLN-PS and PS on oxidative stress in A549 cells using DCFDA, a general RONS probe (24) and MitoSox Red, a mitochondrial superoxide anion ($O_2^{\cdot}$) indicator.

Taking into account the effect of plain SLNs, SLN-PS did not generate increased levels of RONS detected by DCFDA probe compared to PS. Interestingly, SLN-PS increased the amount of mitochondrial superoxide anion by 6-fold over that of the control. Mitochondrial superoxide anion induction was 2-fold higher compared to PS, even when the effect of empty SLNs was subtracted (Fig. 3A). Over-expression of Trx-2, a key protein for redox homeostasis in mitochondria (25), abrogated the induction of mitochondrial superoxide anion and apoptosis by SLN-PS (Fig.3D). This indicates that the increased levels of mitochondrial RONS are critical for the pro-apoptotic effect of SLN-PS.

Given that, compared to PS, SLN-PS triggers profound mitochondrial oxidative stress and $\Delta\psi m$ dissipation, we questioned whether SLN encapsulation can facilitate mitochondrial targeting of PS. Confocal microscopy revealed that SLN-PS started to co-localize with the mitochondria 1 h after incubation with A549 cells, but not in the nucleus (Fig. 3B). Determination of drug levels by HPLC also revealed that compared to PS-treated cells, SLN-PS-treated cells accumulated higher levels of PS in whole cells (3-fold) and mitochondria (4-fold). Indeed, in SLN-PS-treated cells the level of PS in mitochondria was 7.6 times higher than that in whole cell. Such preferential accumulation of PS in mitochondria following treatment with SLN-PS may contribute to its pronounced induction of oxidative stress in mitochondria, compared to PS.

To further substantiate the importance of mitochondrial targeting in the induction of apoptosis by SLN-PS, we generated ρ^0 A549 cells (depleted of mitochondrial DNA). Consistent with our hypothesis, we found that these cells were significantly less sensitive to the pro-apoptotic effects of SLN-PS, with 60 % less cell death compared to A549 cells with the full mitochondrial complement ($1.5\times IC_{50}$; Fig.3 D).

SLN-PS Inhibits the Growth of Human Lung Cancer Xenografts

To assess the *in vivo* efficacy of SLN-PS against lung cancer, we treated nude mice bearing A549 xenografts with vehicle, SLN-PS or PS, starting when the average tumor volume was ~180 mm^3. At dose equivalent to 70% MTD, SLN-PS inhibited profoundly the growth of A549 xenografts, leading to tumor regression during the first 10 days (Fig. 4). By day 16, compared to controls, SLN-PS reduced tumor growth by 78% ($p < 0.005$). In contrast, the effect of PS on the growth of A549 xenograft growth was marginal and did not reach statistical significance.

We next determined cell proliferation and apoptosis in tumor tissue sections. Compared to controls, SLN-PS decreased Ki-67 levels by 71% ($p < 0.001$) and induced apoptosis, increasing it 5.7-fold ($p < 0.01$; Fig. 4). In contrast, PS did not significantly induce apoptosis and only inhibited proliferation modestly (from 61% to 52%, $p < 0.03$). These findings indicate that the profound growth inhibitory effect of SLN-PS is due to its cytokinetic effect.

SLN-PS also significantly induced oxidative stress *in vivo*. As shown in figure 4, urinary level of F2-isoprostane, a marker of oxidative stress, was much higher in SLN-PS-treated group compared to that in the control group. On the other hand, SLN-PS did not increase urinary F2-isoprostane in mice without tumors, suggesting that SLN-PS specifically induced oxidative stress in tumors.

Pharmacokinetics and Biodistribution

Given the remarkable difference in the anti-tumor efficacy between SLN-PS and PS, we assessed their respective pharmacokinetics in mice. *In vivo* PS is rapidly metabolized into several metabolites, of which quantitatively most important are sulindac, sulindac sulfide and sulindac sulfone (7).

Compared to PS, SLN-PS consistently generated higher levels of PS and its three main metabolites in the blood of mice (Fig. 5). PS showed a secondary peak following SLN-PS dosing (i.p.), suggesting the possibility of enterohepatic circulation. The peak levels (C_{max}) of sulindac and sulindac sulfide (>10-fold) after treatment with SLN-PS (i.p.) were much higher than those with PS alone. The total drug levels ($AUC_{0–24h}$ values) obtained with i.p. injection of SLN-PS were 1.8- and 12.4-fold higher than those with oral gavage and i.p. injection of PS, respectively. Our results suggest that SLN encapsulation significantly improves the bioavailability of P-S.

We also compared biodistribution of SLN-PS and PS in the A549 xenografts and major organs in mice (Fig. 5 and Suppl. Fig. 1). Intact PS and PS-sulfone were detected in the A549 xenografts treated with SLN-PS, however, these intact forms were not found after PS administration. Notably, we observed the specific accumulation of intact PS in tumor mitochondria following treatment with SLN-PS (35-fold higher than treatment with PS), suggesting that SLN encapsulation facilitates mitochondrial targeting of PS *in vivo*. Apart from intact PS, the levels of sulindac and sulindac sulfide in A549 xenografts were also much higher (~14-fold) after the administration of SLN-PS. SLN-PS also enhanced drug distribution to the lung and liver, reflecting the higher bioavailability of SLN-PS compared to PS. These data are also in agreement with the *in vitro* cellular uptake study which showed that intracellular levels achieved by SLN-PS were higher than those by PS, even as early as 1 h post dosing (Fig. 3).

The tumor levels of sulindac, sulindac sulfide and sulindac sulfone were significantly associated with tumor volume ($p = 0.003$ to 0.025; Fig. 6), cell proliferation ($p = 0.0001$ to 0.017; Suppl. Fig. 2) and apoptosis ($p = 0.038$ to 0.129, Suppl. Fig 2), with the exception of the correlation between sulindac sulfone and apoptosis. These findings suggests that enhanced efficacy of SLN-PS is closely associated with the improved delivery of PS and its metabolites to the A549 tumors.

DISCUSSION

Our work establishes that incorporating PS in SLNs enhances its efficacy against human lung cancer in pre-clinical models. The superior efficacy of SLN-PS over PS *in vitro* and *in vivo* is due to a constellation of effects: a) a remarkable improvement of PK parameters leading to enhanced delivery of PS to the cancer tissue; b) targeting of SLN-PS to the mitochondria, the master regulator of cell death; and 3) a favorable cytokinetic effect dominated by the activation of the intrinsic apoptosis pathway.

SLN-PS was a much more potent inhibitor of human lung cancer cells than PS and sulindac (over 4- and 44-fold enhancement, respectively), and it exerted a strong inhibitory effect in A549 xenografts. Whereas free PS did not significantly inhibit tumor growth, SLN-PS at an

equivalent dose was remarkably effective, reducing tumor volume by 78 %. A key finding of our study is that SLN-PS exhibits superior PK properties compared to free PS. The phospho-modification of sulindac significantly impacted its physicochemical properties. Most relevant among them is that it increased substantially its hydrophobicity, i.e. it decreased further its already poor water solubility. SLNs, versatile, safe and biocompatible carriers (26), overcame this limitation of PS by solubilizing it, which improved its bioavailability. Incorporation of PS into SLNs led to much higher peak concentrations and $AUCs_{0–24h}$ of PS and its metabolites. More importantly, SLN-PS enhanced by 14-fold the delivery of PS and its metabolites to lung cancer xenografts. In addition to increased bioavailability, it is conceivable that, due to their size (< 100 nm) SLN-PS nanoparticles gained preferential access to tumors though the enhanced permeability and retention effect ("EPR effect" (27)). The higher levels of PS and its metabolites in A549 tumors were consequential, as they correlated with reduced tumor volume, reduced cell proliferation and increased apoptosis. These findings support the idea that the improved delivery of PS to the A549 tumors as a result of its incorporation in SLNs contributes to its efficacy against lung cancer in our tumor model.

Our work also reveals that SLNs potently enhanced the mitochondrial targeting of PS, an effect primarily responsible for the induction of apoptosis *in vitro* and *in vivo*. This is supported by the finding that the SLN formulation increased 35-fold the content of PS in the mitochondria of lung cancer xenografts compared to those from free PS. Enhanced access of PS to mitochondria by SLN formulation occurred in a cell culture system as well, a finding that, in addition, offered a mechanistic window. When we compared free PS to SLN-PS, we obtained two informative sets of responses: although PS alone exhibited preferential accumulation in the mitochondria, SLN-PS generated much higher mitochondrial PS levels and higher rates of apoptosis compared to equimolar amounts of free PS, suggesting that the accumulation of PS in the mitochondria did affect the fate of the cell. This notion was supported by the finding that equipotent (in terms of cytotoxicity) amounts of free PS and SLN-PS generated both similar mitochondrial levels of PS and similar rates of apoptosis. The critical role of mitochondria targeting of PS by SLN-PS in the induction of apoptosis is further confirmed by the observation that mitochondria-deficient (ρ^0) cells were resistant to the cytokinetic effects of SLN-PS.

Mitochondria are a major source of oxidative stress (28) and a central regulator of the intrinsic apoptosis pathway (29). Our data document that, once SLN delivered PS to the mitochondria, PS triggered ROS-dependent cell death. This effect was reflected in a cascade of physicochemical (ROS induction and $\Delta\psi m$ dissipation) and molecular (sequential activation of caspases) changes that culminated in apoptotic cell death. Underlying these changes was the significant induction of superoxide anion levels in the mitochondria in response to PS. A key player here was Trx-2, the Trx isoform predominantly expressed in mitochondria. Trx-2 is part of the Trx system that participates in antioxidant defense; its other members are NADPH and Trx reductase (30,31). Trx-2 plays a crucial role in the scavenging of mitochondrial ROS. In fact, Trx-2 overexpression is cytoprotective against oxidative stress-induced cell death (25,32), whereas its genetic ablation results in massive apoptosis (31). Consistent with this notion, overexpression of Trx-2 in A549 cells completely suppressed the levels of mitochondrial superoxide anion induced by SLN-PS, which was accompanied by dramatically reduced apoptosis. Trx-2 differs markedly in this regard from Trx-1, the other mammalian isoform of Trx, which can enhance or suppress apoptosis depending on biological context (33). Indeed, we have previously demonstrated the pro-apoptotic role of Trx-1 in response to PS (34). Hence, depending on the cellular location that PS is delivered to, the two Trx isoforms may have completely different roles in response to PS induction of cell death. Apart from cellular compartmentation, other factors

such as the redox status of the active site cysteines may also affect the dynamics between Trx and PS (35).

Our data also establish that SLN-PS induced oxidative stress specifically in tumors *in vivo*, by assaying urinary levels of F2-isoprostane. Urinary levels of F2-isoprostanes, derived from non-enzymatic oxidation of arachidonic acid, provide an accurate assessment of oxidative stress *in vivo* (36). SLN-PS-mediated induction of ROS in tumors thus leads to selective killing of cancer cells.

CONCLUSION

Our findings suggest that SLNs are an effective drug delivery system for PS, accounting for the observed therapeutic efficacy of PS against human lung cancer xenografts. The SLN formulation not only improved the PK profile of PS, but was also mitochondrial targeting, which triggered cell death. Given the efficacy of SLN-PS, we speculate that PS, when appropriately formulated, is a promising agent for the treatment of lung cancer that merits further evaluation.

Supplementary Material

Refer to Web version on PubMed Central for supplementary material.

Acknowledgments

We thank the National Institutes of Health National Cancer Institute (R01CA09242308, R01CA139454 and R01CA154172) and the Department of Defense (W81XWH1010873) for financial support of this study.

Basil Rigas has an equity position in Medicon Pharmaceuticals, Inc. and Panayiotis P. Constantinides is affiliated with the same.

ABBREVIATIONS

Δψm	Mitochondrial transmembrane potential
BrdU	5-bromo-2′-deoxyuridine
DCF-DA	2,7-dichlorofluorescein diacetate
NSAIDs	Nonsteroidal anti-inflammatory drugs
NSCLC	Non-small cell lung cancer
PS	Phospho-sulindac
RONS	Reactive oxygen and nitrogen species
SLN	Solid lipid nanoparticles
TUNEL	Deoxynucleotidyl transferase dUTP nick end labeling

REFERENCES

1. Herbst RS, Heymach JV, Lippman SM. Lung cancer. N Engl J Med. 2008; 359(13):1367–1380. [PubMed: 18815398]
2. Haanen C. Sulindac and its derivatives: a novel class of anticancer agents. Curr Opin Investig Drugs. 2001; 2(5):677–683.
3. Malkinson AM. Role of inflammation in mouse lung tumorigenesis: a review. Exp Lung Res. 2005; 31(1):57–82. [PubMed: 15765919]

4. Duperron C, Castonguay A. Chemopreventive efficacies of aspirin and sulindac against lung tumorigenesis in A/J mice. Carcinogenesis. 1997; 18(5):1001–1006. [PubMed: 9163687]
5. Castonguay A, Rioux N. Inhibition of lung tumourigenesis by sulindac: comparison of two experimental protocols. Carcinogenesis. 1997; 18(3):491–496. [PubMed: 9067547]
6. Huang L, Mackenzie G, Ouyang N, Sun Y, Xie G, Johnson F, et al. The novel phospho-non-steroidal anti-inflammatory drugs, OXT-328, MDC-22 and MDC-917, inhibit adjuvant-induced arthritis in rats. Br J Pharmacol. 2011; 162(7):1521–1533. [PubMed: 21175575]
7. Xie G, Nie T, Mackenzie G, Sun Y, Huang L, Ouyang N, et al. The metabolism and pharmacokinetics of phospho-sulindac (OXT-328) and the effect of difluoromethylornithine. Br J Pharmacol. 2011; 165(7):2152–2166. [PubMed: 21955327]
8. Mackenzie GG, Ouyang N, Xie G, Vrankova K, Huang L, Sun Y, et al. Phospho-sulindac (OXT-328) combined with difluoromethylornithine prevents colon cancer in mice. Cancer Prev Res (Phila). 2011; 4(7):1052–1060. [PubMed: 21464038]
9. Huang L, Zhu C, Sun Y, Xie G, Mackenzie GG, Qiao G, et al. Phospho-sulindac (OXT-922) inhibits the growth of human colon cancer cell lines: a redox/polyamine-dependent effect. Carcinogenesis. 2010; 31(11):1982–1990. [PubMed: 20627873]
10. Mackenzie GG, Sun Y, Huang L, Xie G, Ouyang N, Gupta RC, et al. Phospho-sulindac (OXT-328), a novel sulindac derivative, is safe and effective in colon cancer prevention in mice. Gastroenterology. 2010; 139(4):1320–1332. [PubMed: 20600034]
11. Peer D, Karp JM, Hong S, Farokhzad OC, Margalit R, Langer R. Nanocarriers as an emerging platform for cancer therapy. Nat Nanotechnol. 2007; 2(12):751–760. [PubMed: 18654426]
12. Mehnert W, Mader K. Solid lipid nanoparticles: production, characterization and applications. Adv Drug Deliv Rev. 2001; 47(2–3):165–196. [PubMed: 11311991]
13. Uner M, Yener G. Importance of solid lipid nanoparticles (SLN) in various administration routes and future perspectives. Int J Nanomedicine. 2007; 2(3):289–300. [PubMed: 18019829]
14. Zara GP, Cavalli R, Fundaro A, Bargoni A, Caputo O, Gasco MR. Pharmacokinetics of doxorubicin incorporated in solid lipid nanospheres (SLN). Pharmacol Res. 1999; 40(3):281–286. [PubMed: 10479474]
15. Fundaro A, Cavalli R, Bargoni A, Vighetto D, Zara GP, Gasco MR. Non-stealth and stealth solid lipid nanoparticles (SLN) carrying doxorubicin: pharmacokinetics and tissue distribution after i.v. administration to rats. Pharmacol Res. 2000; 42(4):337–343. [PubMed: 10987994]
16. Zara GP, Cavalli R, Bargoni A, Fundaro A, Vighetto D, Gasco MR. Intravenous administration to rabbits of non-stealth and stealth doxorubicin-loaded solid lipid nanoparticles at increasing concentrations of stealth agent: pharmacokinetics and distribution of doxorubicin in brain and other tissues. J Drug Target. 2002; 10(4):327–335. [PubMed: 12164381]
17. Reddy LH, Adhikari JS, Dwarakanath BS, Sharma RK, Murthy RR. Tumoricidal effects of etoposide incorporated into solid lipid nanoparticles after intraperitoneal administration in Dalton's lymphoma bearing mice. AAPS J. 2006; 8(2):E254–262. [PubMed: 16796375]
18. Jain SK, Chaurasiya A, Gupta Y, Jain A, Dagur P, Joshi B, et al. Development and characterization of 5-FU bearing ferritin appended solid lipid nanoparticles for tumour targeting. J Microencapsul. 2008; 25(5):289–297. [PubMed: 18608808]
19. Arias JL, Clares B, Morales ME, Gallardo V, Ruiz MA. Lipid-based drug delivery systems for cancer treatment. Curr Drug Targets. 2011; 12(8):1151–1165. [PubMed: 21443475]
20. Kozoni V, Tsioulias G, Shiff S, Rigas B. The effect of lithocholic acid on proliferation and apoptosis during the early stages of colon carcinogenesis: differential effect on apoptosis in the presence of a colon carcinogen. Carcinogenesis. 2000; 21(5):999–1005. [PubMed: 10783324]
21. Naito A, Carcel-Trullols J, Xie CH, Evans TT, Mizumachi T, Higuchi M. Induction of acquired resistance to antiestrogen by reversible mitochondrial DNA depletion in breast cancer cell line. Int J Cancer. 2008; 122(7):1506–1511. [PubMed: 17990320]
22. Newmeyer DD, Ferguson-Miller S. Mitochondria: releasing power for life and unleashing the machineries of death. Cell. 2003; 112(4):481–490. [PubMed: 12600312]
23. Circu ML, Aw TY. Reactive oxygen species, cellular redox systems, and apoptosis. Free Radic Biol Med. 2010; 48(6):749–762. [PubMed: 20045723]

24. LeBel CP, Ischiropoulos H, Bondy SC. Evaluation of the probe 2',7'-dichlorofluorescin as an indicator of reactive oxygen species formation and oxidative stress. Chem Res Toxicol. 1992; 5(2):227–231. [PubMed: 1322737]
25. Tanaka T, Hosoi F, Yamaguchi-Iwai Y, Nakamura H, Masutani H, Ueda S, et al. Thioredoxin-2 (TRX-2) is an essential gene regulating mitochondria-dependent apoptosis. EMBO J. 2002; 21(7): 1695–1703. [PubMed: 11927553]
26. Attama AA. SLN, NLC, LDC: State of the Art in Drug and Active Delivery. Recent Pat Drug Deliv Formul. 2011; 5(3):178–187. [PubMed: 21834777]
27. Maeda H, Bharate GY, Daruwalla J. Polymeric drugs for efficient tumor-targeted drug delivery based on EPR-effect. Eur J Pharm Biopharm. 2009; 71(3):409–419. [PubMed: 19070661]
28. Fulda S, Galluzzi L, Kroemer G. Targeting mitochondria for cancer therapy. Nat Rev Drug Discovery. 2010; 9(6):447–464.
29. Kroemer G, Galluzzi L, Brenner C. Mitochondrial membrane permeabilization in cell death. Physiol Rev. 2007; 87(1):99–163. [PubMed: 17237344]
30. Holmgren A, Lu J. Thioredoxin and thioredoxin reductase: current research with special reference to human disease. Biochem Biophys Res Comm. 2010; 396(1):120–124. [PubMed: 20494123]
31. Nonn L, Williams RR, Erickson RP, Powis G. The absence of mitochondrial thioredoxin 2 causes massive apoptosis, exencephaly, and early embryonic lethality in homozygous mice. Mol Cell Biol. 2003; 23(3):916–922. [PubMed: 12529397]
32. Hansen JM, Zhang H, Jones DP. Mitochondrial thioredoxin-2 has a key role in determining tumor necrosis factor-alpha-induced reactive oxygen species generation, NF-kappaB activation, and apoptosis. Toxicol Sci. 2006; 91(2):643–650. [PubMed: 16574777]
33. Zhang R, Al-Lamki R, Bai L, Streb JW, Miano JM, Bradley J, et al. Thioredoxin-2 inhibits mitochondria-located ASK1-mediated apoptosis in a JNK-independent manner. Circ Res. 2004; 94(11):1483–1491. [PubMed: 15117824]
34. Sun Y, Rigas B. The thioredoxin system mediates redox-induced cell death in human colon cancer cells: implications for the mechanism of action of anticancer agents. Cancer Res. 2008; 68(20): 8269–8277. [PubMed: 18922898]
35. Kozoni V, Rosenberg T, Rigas B. Development of novel agents based on nitric oxide for the control of colon cancer. Acta Pharmacol Sin. 2007; 28(9):1429–1433. [PubMed: 17723176]
36. Milne GL, Sanchez SC, Musiek ES, Morrow JD. Quantification of F2-isoprostanes as a biomarker of oxidative stress. Nat Protoc. 2007; 2:221–226. [PubMed: 17401357]

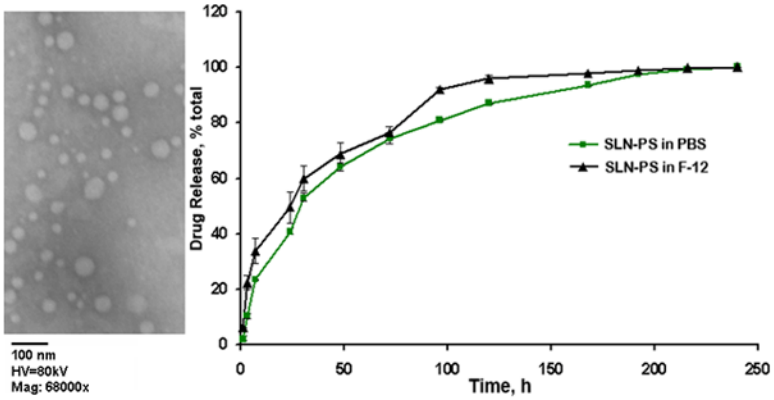

IC_{50}, μM	Sulindac	PS	SLN-PS
A549	>1000	88 ± 15	23 ± 5
Enhancement over sulindac		*>11*	*>44*
Enhancement over PS			*4*
H510	>1000	45 ± 7	9 ± 4
Enhancement over sulindac		*>22*	*>111*
Enhancement over PS			*5*

Fig. 1. SLN-PS: Characterization and effect on cell growth

SLN-PS nanoparticles were evaluated by TEM (*upper left*); their average size is ~55 nm. The cumulative release of PS from SLN-PS into PBS (pH 7.4) or F-12K cell culture medium was monitored for 240 h (*upper right*); drug levels were determined by HPLC as in Methods. The Table summarizes the 24-h IC_{50} of sulindac, PS and SLN-PS in two lung cancer cell lines.

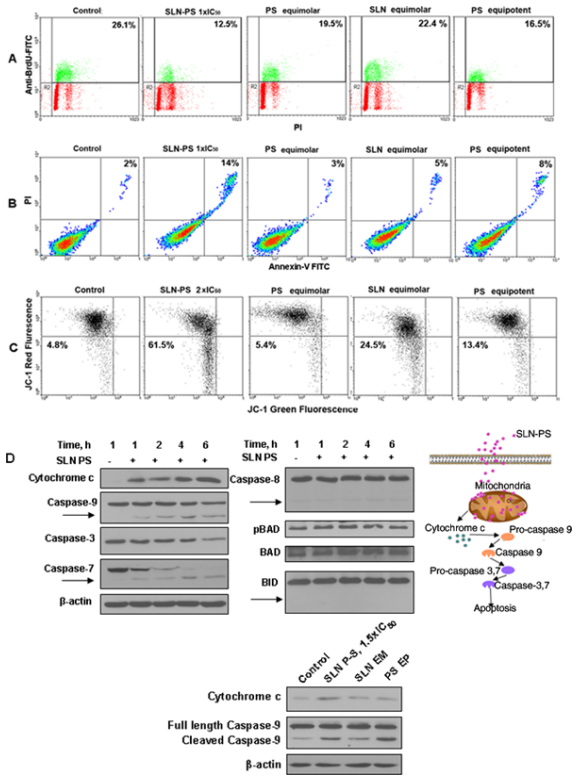

Fig. 2. The effect of SLN-PS on cytokinetics and mediators of apoptosis in A549 lung cancer cells

Cells were treated with SLN-PS or PS (equimolar or equipotent to SLN-PS in terms of cell growth inhibition) or plain SLNs (no drug loaded) equivalent to SLN-PS. **A:** Cell proliferation was determined by BrdU incorporation after 6 h treatment with the test compounds. Numbers indicate the percentage of cells in S phase. **B:** Apoptosis was determined by flow cytometry in cells stained with Annexin-V (abscissa) and PI (ordinate). Apoptotic cells are in the right upper quadrant; their proportion of the total is indicated as a percentage. **C:** Mitochondrial transmembrane potential ($\Delta\psi m$) was determined using the molecular marker JC-1; increased JC-1 green fluorescence indicates decreased $\Delta\psi m$. **D:** Immunoblots of various proteins involved in the apoptosis cascade. A549 cells were treated with SLN-PS for the indicated time periods and SLN-PS, SLNs or PS for 4 h. Arrows: products of hydrolytic cleavage of the corresponding (pro)caspase. These findings establish the activation of the intrinsic apoptosis pathway, shown diagrammatically on the right.

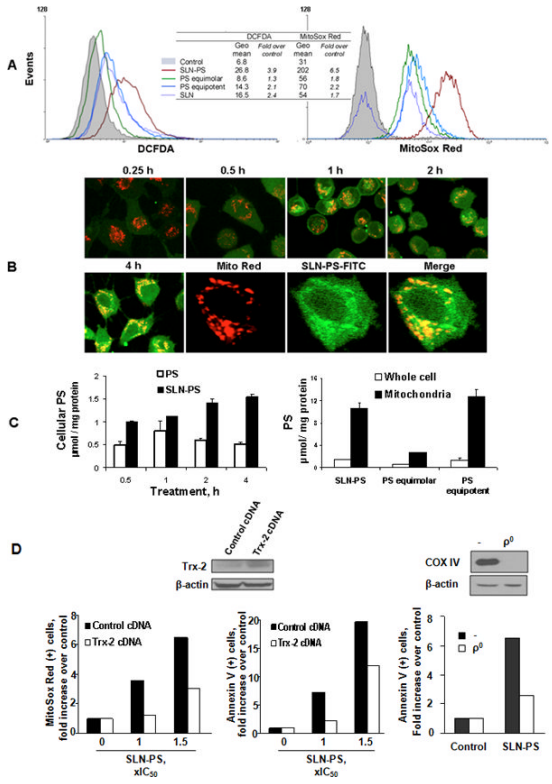

Fig. 3. The effect of SLN-PS on ROS levels and its uptake by A549 cells

A: *Left*: ROS levels in A549 cells treated as in Methods for 1 h with SLN-PS 1×IC_{50}, SLNs (equivalent) or PS (equimolar or equipotent). Cells were preloaded with the fluorescent molecular probe DCFDA and examined by flow cytometry. *Right:* A549 cells were treated with SLN-PS 2×IC_{50}, SLNs (equivalent) or PS (equimolar or equipotent) preloaded with MitoSOX Red, which detects mitochondrial $O_2^{\cdot}$ and its fluorescence was determined by flow cytometry. **B:** SLN-PS was loaded with FITC (green fluorescence) as in Methods and A549 cells were treated with SLN-PS-FITC 2×IC_{50} for the indicated time periods. The uptake of SLN-PS was monitored by confocal microscopy. Cells were also pretreated with Mitotracker Red (red fluorescence), a mitochondrion-selective fluorescent probe. Yellow/orange color arises when SLN-PS-FITC is present in the mitochondria (co-localisation). **C:** *Left*: Concentration of PS in A549 cells treated with equimolar amounts of SLN-PS or PS at 1–4 h following addition of the drug to the culture medium. *Right*: Mitochondrial concentration of PS in A549 cells treated with SLN-PS or PS for 2 h. Values are mean±SD (quadruplicate experiments). **D:** *Left*: A549 cells overexpressing Trx-2 were treated with SLN-PS 0, 1, 1.5×IC_{50} preloaded with MitoSOX Red (detects mitochondrial $O_2^{\cdot}$) and fluorescence was determined by flow cytometry. *Middle*: Trx-2 overexpressed A549 cells were treated with SLN-PS 0, 1, 1.5×IC_{50} preloaded with Annexin-V and PI, determined by flow cytometry. *Right*: MtDNA-less A549 cells were treated with SLN-PS 1.5×IC_{50} preloaded with Annexin-V and PI, analysed by flow cytometry.

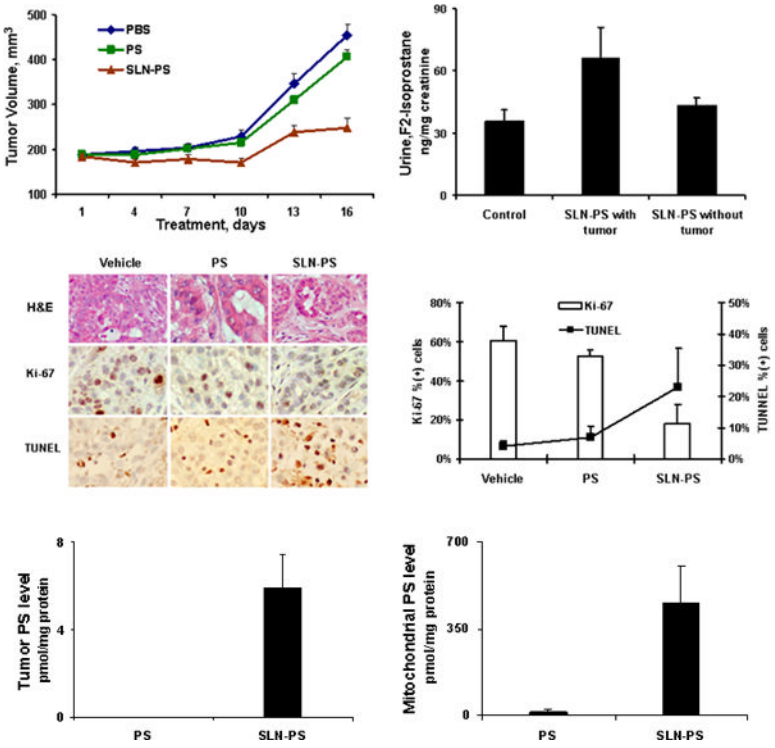

Fig. 4. Xenografts inhibitory effect and *in vivo* immunostaining

Upper Left: the inhibitory efficacy on tumor growth of SLN-PS and PS. *Upper Right*: urinary F2-isoprostane levels of nude mice bearing/not bearing A549 xenografts treated with SLN-PS. *Middle Left*: H&E, Ki-67 and TUNNEL in tissue sections from A549 xenografts. *Middle Right*: the quantification of expression of Ki-67 and TUNNEL based on the number of positive cells. *Lower Right*: Drug levels of PS from the A549 xenografts. *Lower Left*: Drug levels of PS from the mitochondria of A549 xenografts.

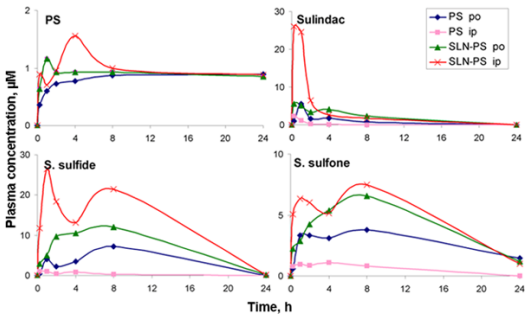

Plasma Levels of PS and Metabolites
AUC (arbitrary units), (% total)

	PS	Sulindac	S.sulfide	S.sulfone
		Oral		
PS	900 (7)	1,862 (14)	6,033 (46)	4,404 (33)
SLN-P-S	1,170 (5)	4,779 (21)	10,352 (45)	6,899 (30)
		Intraperitoneal		
PS	1,101 (39)	332 (12)	433 (15)	950 (34)
SLN-P-S	1,332 (4)	6,854 (20)	18,481 (53)	8,384 (24)

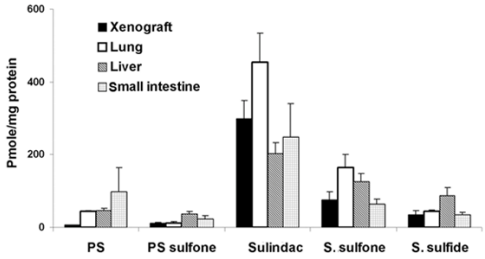

Fig. 5. Pharmacokinetics of PS and its metabolites in mouse plasma and its biodistribution after treatment with PS or SLN-PS

(A) Pharmacokinetic curves of PS and its metabolites after treatment with PS or SLN-PS via p.o. or i.p. in 24 h. (B) AUC value of PS and its metabolites after treatment with PS or SLN-PS via p.o. or i.p. (C) Drug level of PS and its metabolites in different organs after treatment with SLN-PS via i.p. (Biodistribution of PS and its metabolites after treatment with PS is shown in Suppl. Fig. 1).

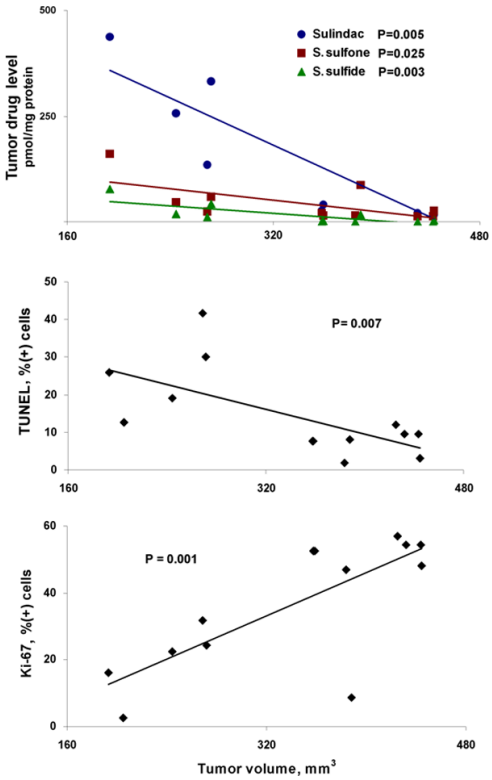

Fig. 6. Correlation between antitumor effect with tumor drug level and Ki-67 or TUNEL positive cell ratio

Upper panel, sulindac, s. sulfide and s. sulfone tumor levels correlations with tumor volume, all of them have significant correlations with antitumor effect; Middle panel, ratio of TUNEL positive cell is adversely correlated with tumor volume; Lower panel, ratio of Ki-67 positive cells is significantly correlated with tumor volume.